Updates to Simulation of a Single-Element Lean-Direct Injection Combustor Using Arbitrary Polyhedral Meshes

Thomas Wey[1] and Nan-Suey Liu[2]

NASA Glenn Research Center

Cleveland, Ohio 44135 USA

Abstract

This paper summarizes the procedures of (1) generating control volumes anchored at the nodes of a mesh; and (2) generating staggered control volumes via mesh reconstructions, in terms of either mesh realignment or mesh refinement, as well as presents sample results from their applications to the numerical solution of a single-element LDI combustor using a releasable edition of the National Combustion Code (NCC).

Introduction

The lean direct injection (LDI) concept has the potentials for low gaseous and particulate emissions as well as less auto-ignition under operational (compression ratios up to 60:1 and peak flame temperature 3000°F) conditions. For a LDI combustor, most of the air directly enters the combustor through the swirler. In this concept, the liquid fuel is injected from fuel injectors directly into the incoming swirling airflow, and the swirling air stream is used to atomize the injected liquid as well as to promote fuel-air mixing. The flame structure can be very complex and locally range from non-premixed to premixed burning.

Recently, a single-element LDI combustor experiment has been used as a test bed for assessing, further developing and validating the capability of two-phase turbulent combustion modeling and simulation. This combustor consists of an air passage with a sixty-degree six-bladed air swirler, a converging-diversion section and a chamber with a square cross-section. The fuel is injected through the center of the swirler and exit at the throat of the venture.

A series of numerical calculations have been performed by using (1) the time filtered Navier-Stokes (TFNS) methodology and (2) the large eddy simulation (LES)

[1] Research Aerospace Engineer, Engine Combustion Branch.
[2] Research Aerospace Engineer, Engine Combustion Branch, Associate Fellow AIAA.

methodology. The sub-grid models employed for turbulent mixing and combustion include the well-mixed model, the linear eddy mixing (LEM) model; the Eulerian filtered mass density function (EUFDF/EUPDF) model, and the flamelet-based model. Results from these methodologies invoking various sub-grid models are summarized in Reference [1], and a more detailed description of the TFNS approach can be found in Reference [2] and [3]. It should be pointed out that TFNS is not LES, nor hybrid RANS/LES, nor, in general, unsteady Reynolds-averaged Navier-Stokes (URANS). Like the LES, TFNS is capable of capturing the dynamically important, unsteady turbulent flow structures, even when RANS-grade meshes are used. Unlike the LES, the grid resolution and the turbulence model fidelity are not formally linked, therefore, in principle; a grid independent solution can be unambiguously attained in the TFNS approach.

Both of the turbulence-chemistry sub-grid models mentioned above do not solve components of the momentum in the sub-grid elements or particles. In addition to the physics-based sub-grid models for the entire domain, an *adaptive* mesh-based sub-grid model was developed and implemented recently.

In previous work [4], a mesh-based enhancement for the scalar mixing was proposed. It was speculated there that greater number of the flux-exchange between solution elements, i.e. using polyhedrons as control volumes, may have the potentials to enhance the mixing of the scalar for the modeling of the turbulence-chemistry interaction. In that work, a honeycomb like polyhedral mesh was generated from a regular unstructured mesh, which could be the combinations of tetrahedrons, hexahedrons, prisms and pyramids, through the processes of refinement, reconnection and agglomeration.

In Ref. [5], a polyhedral mesh is generated or more precisely post-processed from a set of hanging-node or conforming unstructured mesh. Those sub-grid refinements are done in all directions for the selected cells. For the cases of high Reynolds number flows, the sub-grid refinements normal to wall are desirable and necessary. It is well known that inviscid tetrahedral mesh or hanging-node mesh, such as Cartesian mesh, can be generated very quickly with minimal user interfaces. They are ideal for the rapid prototyping of the combustor geometry. However in most of cases, those meshes are not suitable for the high Reynolds number turbulent flows due to lack of well-behaved layer mesh near the walls. Even in the conceptual design stages of the combustors, the viscous effects of the solid walls should be treated as one of the design variables. In Ref. [6], a thin-layer, normal to wall refinement scheme is developed to enable an originally inviscid grid suitable for high Reynolds number flows.

The honeycomb-like polyhedral mesh discussed in Ref. [4] actually increases the number of control volumes. Nevertheless it is also known that the tetrahedral mesh can be generated very quickly with minimal user interfaces, hence they are ideal for the rapid prototyping of the combustor geometry.

To further reduce the time needed in the conceptual design stages of the combustors, users may want to have the option to store the unknowns at the nodes of a given

tetrahedral mesh for the purpose of down-select the final geometry because number of the nodes is much smaller than that of the cells in a tetrahedral mesh. In the first part of the present work, a polyhedron mesh generation technique is introduced in order to reduce the initial design cost of the desired geometry of the combustors. Less unknowns use less CPU time. However, less number of solution elements in a given domain may have adverse effects on drag, temperature and scalar mixing, etc.

To predict better drag, hear transfer and scalar mixing, high-order CFD methods have received considerable attention recently. To achieve the goal of higher order accuracy, the divergence theorem is re-interpreted from the point of view of mesh reconstruction. In the second part of the present work, a polyhedron mesh generation technique is introduced in order to introduce high order scheme into the code used for time filtered Navier-Stokes (TFNS) approach. It is further noted here that similar overlapping control volume configuration in the present work has been used by one of spatial test filters required in the popular dynamic models of large-eddy simulations.

The main purposes of this report are to describe the practical aspects of the generation of the arbitrary polyhedral mesh and their application.

Generation of Polyhedrons via Node-Based Control Volume of a Mesh

The process starts by computing a nominal centroid for each cell of the original mesh. The nominal centroids could be typical geometry centroids or circumscribe centroids. A loop formed by the connecting surrounding nominal centroids of an edge defines a polygon. Then, agglomeration of those polygons forms a polyhedron anchored at the nodes of the original mesh, see Figures 1 and 2 for examples.

Some polyhedrons at the corners of the boundary faces could be concave, such as near trailing edges of the rotor blades. Concave polyhedrons will create issues for the routines that are related to the turbulence modelling and the search of the spray droplets. The centroid is calculated differently for concave and convex polyhedrons. In the present work, the centroid, geometric center, of the cell is used as the solution centre for a convex polyhedron. For a concave polyhedron, the centroid of the visible region of the cell is used as the solution centre. The visible region of the cell is defined as the union of the points that is visible from any point on the boundary of the cell and vice versa, i.e. it can see any point on the boundary. Based upon this visibility restriction, any ray from the boundary of the cell to the visible solution centre will not intersect with any other boundary and any droplet contained by this concave cell can be detected easily. The normal distance from the wall surface to the solution centre is always positive which is essential for the turbulence wall function calculation.

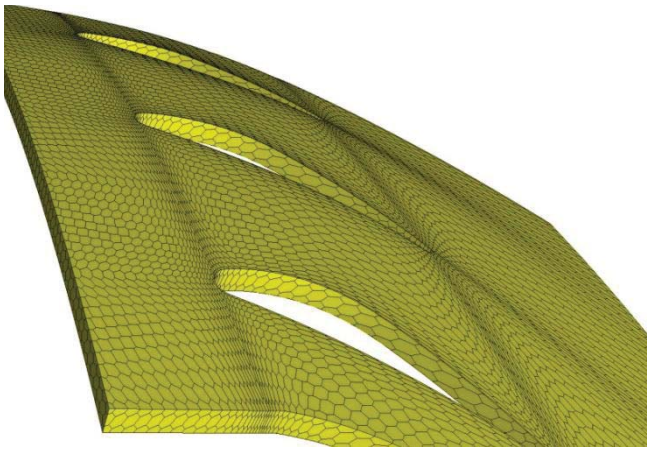

Figure 1 Boundary polygons of a polyhedron generated from a set of all-tetrahedron rotor mesh.

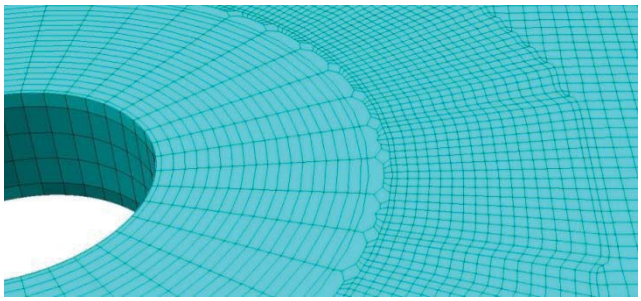

Figure 2 Partial boundary polygons are shown; Polyhedrons are generated from a combination of hexahedrons, tetrahedrons and pyramids.

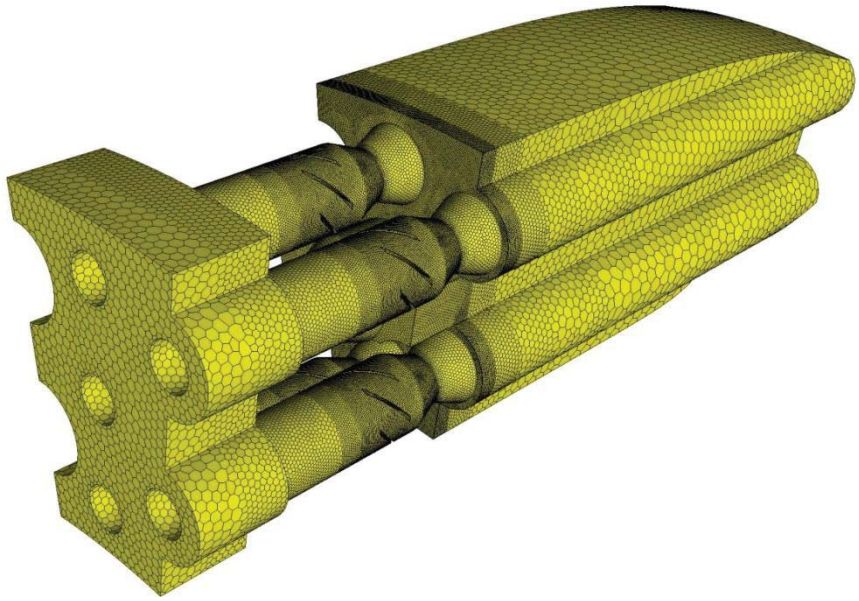

Figure 3 Partial boundary polygons are shown; Polyhedrons are generated for a conceptual N+3 LDI combustor

Domain decomposition is a very important subject for the massive parallel computations. Especially the number of faces in an arbitrary polyhedron mesh is much greater than that of a regular unstructured mesh. METIS 4.0.1, freely available software from University of Minnesota, is used to partition the domain of the computation. METIS 4.0.1 currently supports only four basic element types: triangles, quadrilaterals, tetrahedrons, and hexahedrons but it does not support arbitrary polyhedrons. Fortunately, PARTDMESH in METIS 4.0.1 will produce both a list of the elements belonging to each part of the partition, and a list of the nodes belonging to each associated part of the pseudo-partition of the nodes. Since the first type of polyhedral mesh utilizes nodes of the original mesh, the final list of partition information for the polyhedral mesh is acquired.
An all-tetrahedron mesh describing a conceptual N+3 LDI combustor is selected for the demonstration. The original mesh contains 5,162,593 tetrahedrons, 926,030 nodes and 10,466,807 faces. The face-to-cell ratio is about 2.03. The derived polyhedral mesh contains 926,030 polyhedrons, 5,468,290 nodes and 6390,318 faces. The face-to-cell ratio jumps to 6.9 which represent a large increase of flux exchange per control volume. In Figure 3, the boundary polygons of the combustor are shown.

Generation of Polyhedrons via Overlapping Control Volume of a Mesh

It is well known that the divergence theorem is one of the fundamental tools of the finite volume methods for CFD. The divergence theorem relates the volume integrals and the surface integrals. For example, the species transport equation in multiple rotating frames of reference (MRF) is written as:

$$\frac{d}{dt}\iiint_V \rho_m \, dV + \iint_A \rho_m (\vec{u} - \vec{U}_g) \cdot d\vec{A} = \iint_A \rho D_{eff} \nabla(\frac{\rho_m}{\rho}) \cdot d\vec{A} + \iiint_V \dot{w}_m''' dV + \iiint_V S_{mls} dV \quad (1)$$

$\dot{w}_m'''$, the production rate of species m per unit volume, is the main source of the turbulence-chemistry interaction. S_{mls} is the source term due to the contribution of spray. There are two surface integrations in which the unknowns on surfaces and surface area vectors are required. Most numerical schemes are designed to reconstruct the unknowns, located in centroids of the volumes, to be on the surfaces and then perform the integration afterwards. In the present work, instead of flux or unknown reconstructions, the facets of the mesh are reconstructed such that the facets of the control volumes pass through the centroids of the meshes. Two approaches of the mesh reconstructions are considered. One is achieved via mesh realignment; the other is via full mesh refinement.

1. Mesh Realignment Approach

The process of generating an overlapping control volume starts by constructing a three-point control surface from geometric center of a cell, or a circumsphere center of certain well behaved tetrahedron, to each edge in the cell. It is equivalent to splitting a cell into smaller sub-cells such that the number of sub-cells is equal to the number of faces and each face of the cell is associated with a sub-cell. Reconnection and agglomeration are

applied to each cell such that each cell has additional sub-cells which are provided or donated by adjacent cells. In Figure 4, a cell is depicted by adding a sub-cell of the adjacent cell to the host cell. A rule of thumb to compute the fluxes and gradients is that unknowns and their derivatives at "cell 4" is used for integration at "facet i". Damping is added via differencing of unknowns at "cell 5" and "cell 7" for "facet i". In the present work, the fourth order damping is always turned on, however the second order damping is adaptively added only if it is needed in the high gradient regions. The mechanism to add second order damping or not is similar to traditional shock-capturing limiters. However, the mesh-realignment approach has the potential to generate the control volumes contained very small acute angles if the aspect ratios of the original mesh are large.

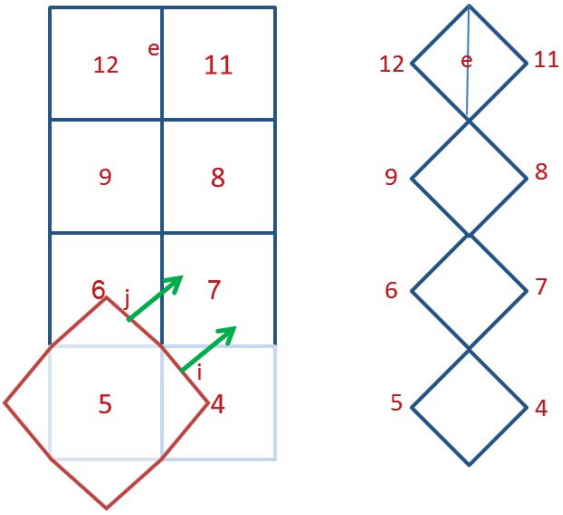

Figure 4 Schematic illustrating the mesh realignment process used for generating overlapping control volumes.

In Figure 5, control volume, **a**, is surrounded by two groups of control volumes. Control volumes of the first group marked as **b, c, d** and **e** are the ones adjacent to **a** that the fluxes are exchanged between them. Control volumes of the second group marked as, **P, Q, R, S** are the ones overlapped with **a**. The integration point, **x**, is on the control surface of **a** whose variables are extrapolated from **P**. A three-dimensional third-order Taylor series expansion formula is applied to $\vec{x}$ from $\vec{P}$ to compute all necessary variables at the integration points for the fluxes computations:

$$U(\vec{x}) = U(\vec{P}) + U'(\vec{P})(\vec{x} - \vec{P}) + \frac{1}{2}U''(\vec{P})(\vec{x} - \vec{P})^2 + \frac{1}{6}U'''(\vec{P})(\vec{x} - \vec{P})^3,$$

Similarly, a second-order Taylor series expansion for any variable at **x** will look like:

$$U(\vec{x}) = U(\vec{P}) + U'(\vec{P})(\vec{x} - \vec{P}) + \frac{1}{2}U''(\vec{P})(\vec{x} - \vec{P})^2,$$

In this way, higher than second order accuracy for TFNS approach can be achieved.

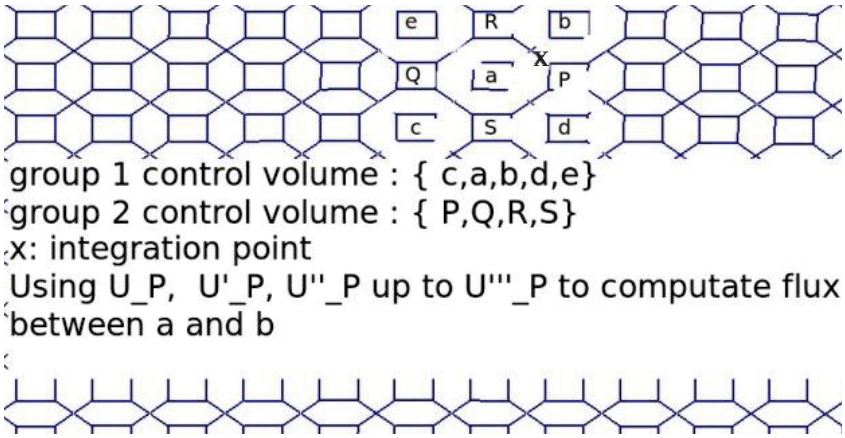

Figure 5 Illustrating Taylor series expansion formula from $\vec{P}$ to $\vec{x}$, integrating point.

Mesh realignments result in staggered overlapping control volumes. Reconstructions of the unknown vectors from the centroids to the facets are avoided. High order accuracy can be achieved easier. In Figures 6 and 7, overlapping control volumes generated from hanging-node polyhedrons are shown.

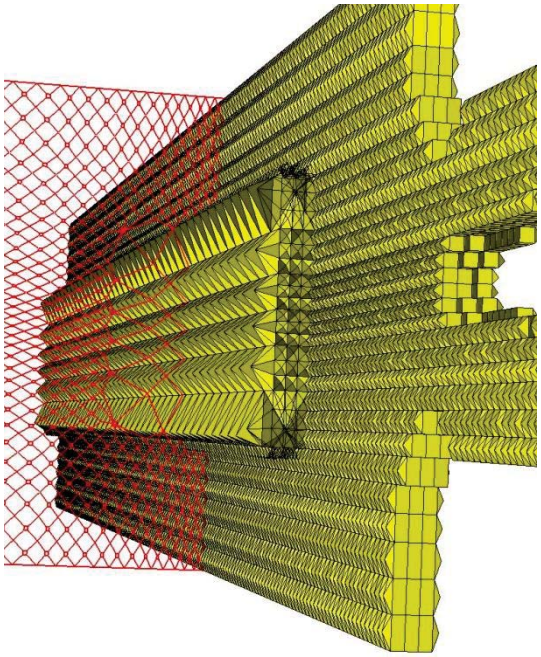

Figure 6 Example of control volumes derived from hanging-node polyhedrons.

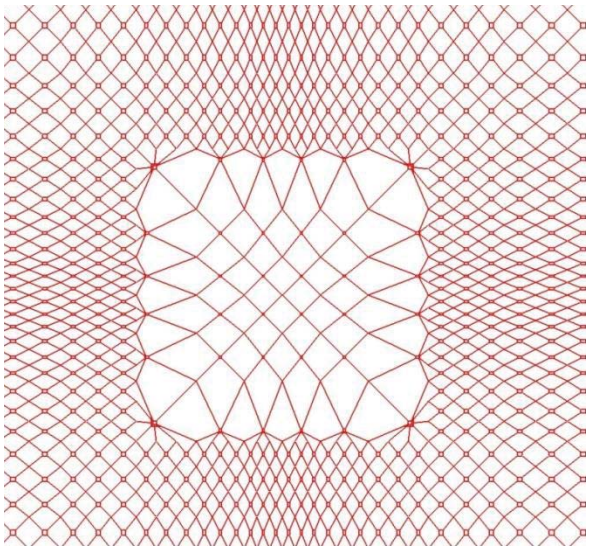

Figure 7 A slice of an overlapping control volumes by mesh realignment process.

2. Mesh Refinement Approach

To avoid small acute angles, second approach to introduce here. A quad-tree or oct-tree refinement of each cell is performed such that newly created facets pass through the centroids of the mesh cells. New unknown vectors are added to newly created control volumes. It is equivalent that for a given mesh, the solutions are stored at the centroids and the nodes of the original meshes.

The rule of thumb to compute the fluxes and gradients is that unknowns and their derivatives at "cell 6" is used for integration at "facet i", see Figure 8.

The fourth order damping is always turned on; however the second order damping is adaptively added only if lower order accuracy is needed for high gradient regions.

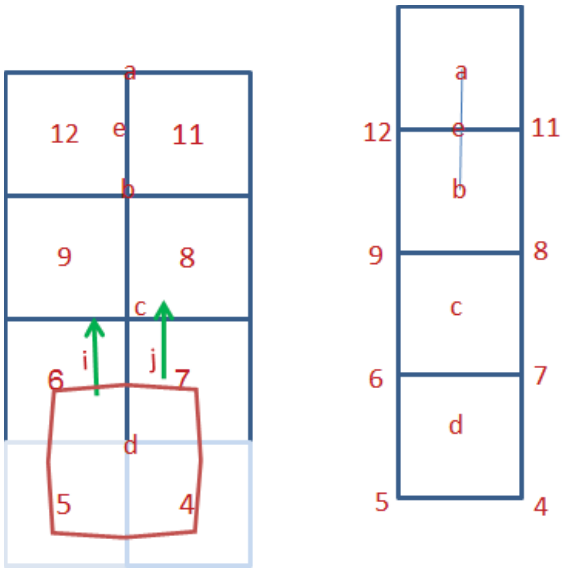

Figure 8 Schematic illustrating the mesh refinement process used for generating overlapping control volumes.

Mesh refinements result in staggered overlapping control volumes too.
Reconstructions of the unknown vectors from the centroids to the facets are avoided.
High order accuracy can be achieved easier.

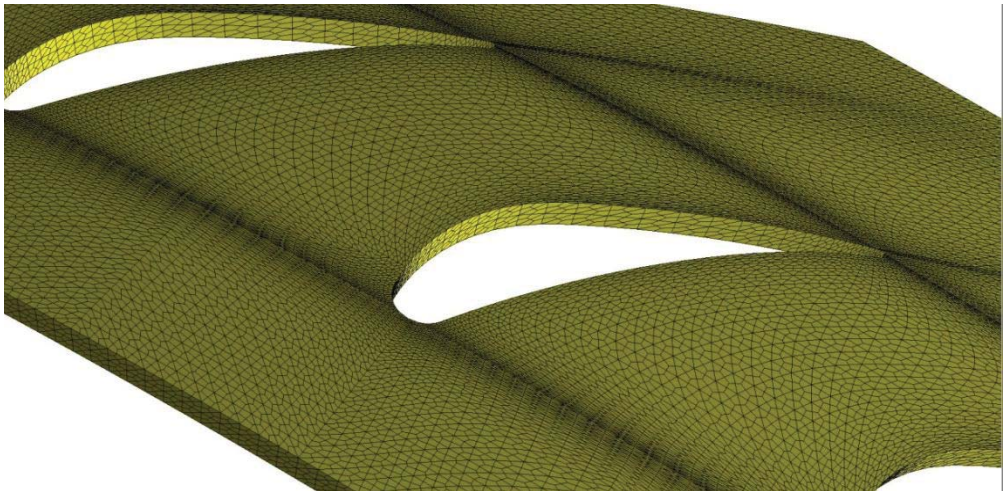

Figure 9 Boundary faces of an overlapping control volume by mesh refinement process.

Domain decomposition for overlapping control volumes is more complicated than that for non-overlapping control volumes. Since each facet of an overlapping control volume must carry three bits of information: two adjacent control volumes and one unknown-providing control volume. It increases the number of messages passed between the partitions greatly. Besides the issue of message passing, the search algorithm of the spray droplets needs to be modified to be able to deal with the ambiguity of the overlapping. It

increases the time needed for searching for droplets. Another important issue is the existence of the concave control volumes which also increase the computing time for the simulations. In this paper, only the results of the mesh-realignment approach will be reported. It needs to be emphasised here that the overlapping control volume scheme is not the same as the popular overset grid scheme.

Preliminary Non-Reacting Results

Sample Applications of Using Mesh-Node-Based Control Volumes

An all-tetrahedron mesh describing a single-element LDI combustor is selected for the demonstration. The original mesh contains 1,554,419 tetrahedrons, 283,200 nodes and 3,158,261 faces. The face-to-cell ratio is about 2.03. The derived polyhedral mesh contains 283,200 polyhedrons, 1,699,188 nodes and 1,952,377 faces. The face-to-cell ratio jumps to 6.89 which represent a large increase of flux exchange per control volume. In Figures 4 the boundary polygons are shown.

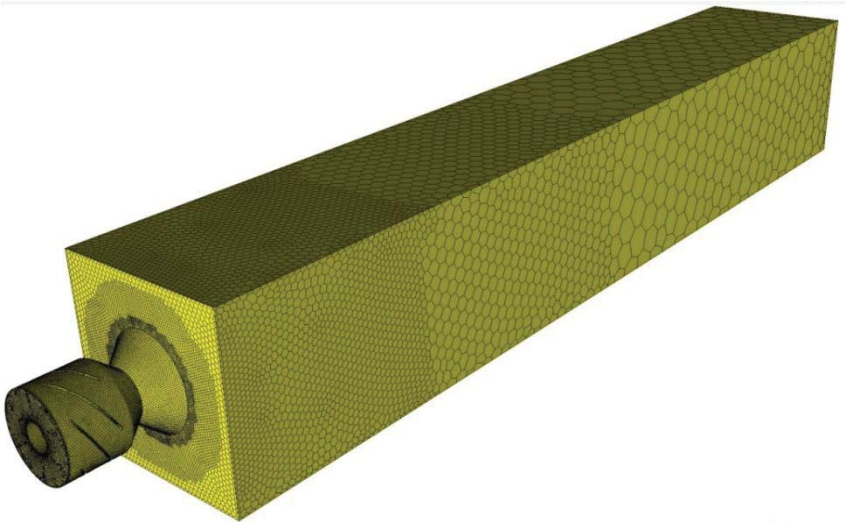

Figure 10 Boundary polygons of the combustor.

Both the original mesh and the derived polyhedrons are used for the simulations.
At the inlet, the inflow velocity, the static temperature and the density of the gas phase are specified as 20.14 m/s, 294.28 K, 1.19 kg/m^3 respectively. At the outflow boundary, the static pressure is imposed at 101325 Pa. The generalized wall function is applied to solid wall boundaries. The thermal boundary condition for all the solid surfaces of the combustor is set to be adiabatic. Both simulations are executed for the non-reaction RANS case. Figure 11 to 12 are for the case of original mesh. Computed axial velocity on a plane around z=0 is shown in Figure 11. The pressure contours on a plane at z=0 is shown in Figure 12. Low pressure center can be seen very clearly.

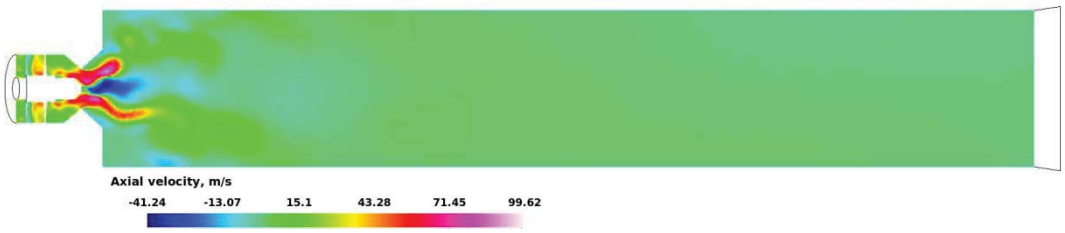

Figure 11 Axial velocity contours at z=0 plane (i.e. mid plane) of original mesh.

Figure 12 Pressure contours at z=0 plane of original mesh.

For the case with the polyhedrons, control volumes, axial velocity contours, and pressure contours are shown Figure 13 to 15.

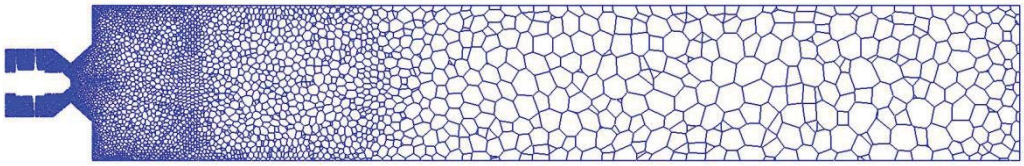

Figure 13 A plane cut of polyhedrons around the mid-plane of the combustor

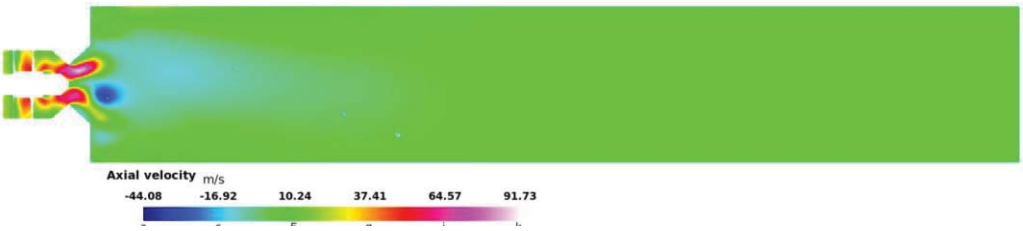

Figure 14 Axial velocity contours at z=0 plane (i.e. mid plane) of polyhedral mesh.

Figure 15 Pressure contours at z=0 plane of polyhedral mesh.

While the number of control volumes in derived polyhedral mesh is about 18% of the original mesh, the number of faces in derived polyhedral mesh is about 62% of the original mesh. For non-reacting case, the CPU time saved is merely around 50%. For reacting case, it is expected that the saving in CPU time will be much larger, since the

source terms of the species transport equations are dependent on the number of control volumes.

Sample Applications of Using Overlapping Control volumes

Benchmark case of Laminar Flow – a Flat Plate

A set of adaptively refined quadrilateral mesh, shown in Figure 16, is generated for a flat plate. The derived overlapping control volumes are shown in Figure 17. The simulations are performed such that the second order scheme is applied to former grid, while the third order scheme is applied to latter grid. The numerical solutions are benchmarked against the theoretical results and empirical formula available. In Figure 19, the skin coefficient by the third order scheme is much more closer to the theoretical value than that of the second order scheme. In Figure 20, the heat transfer coefficients show very similar behavior.

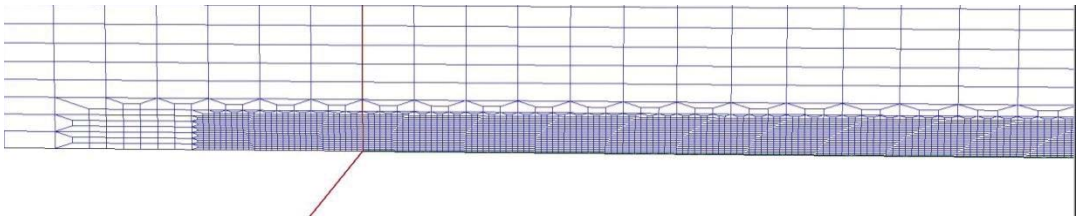

Figure 16 3h adaptively refined quadrilateral mesh for a flat plate.

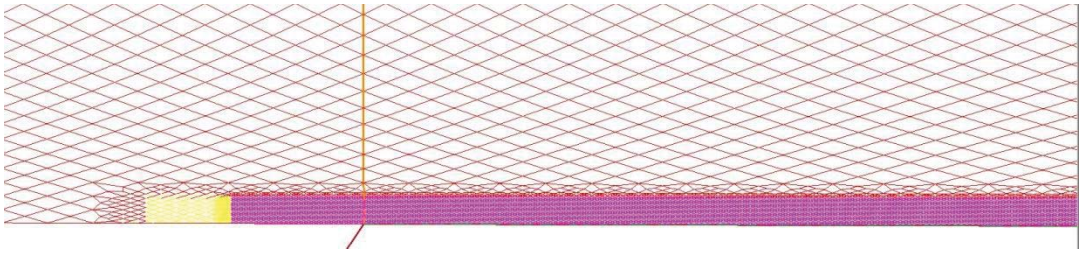

Figure 17 Overlapping control volume derived from Figure 16.

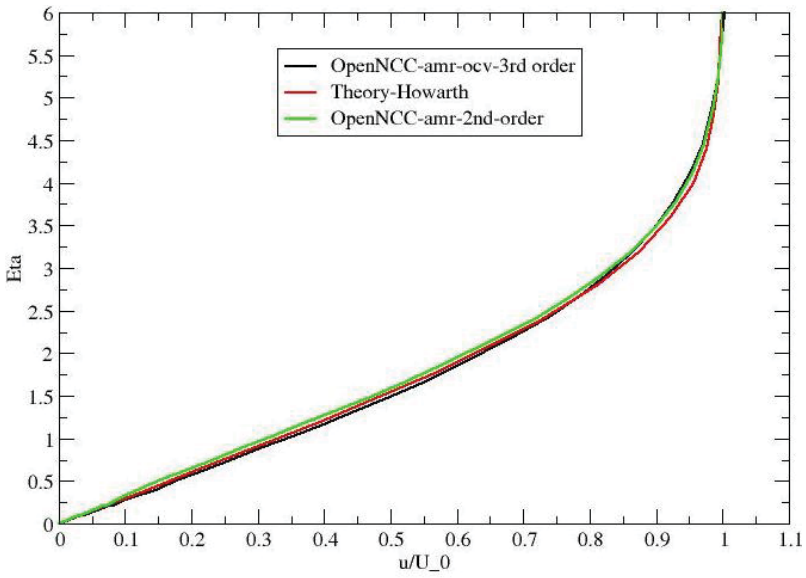

Figure 18 Dimensionless velocity profiles at the end of the domain.

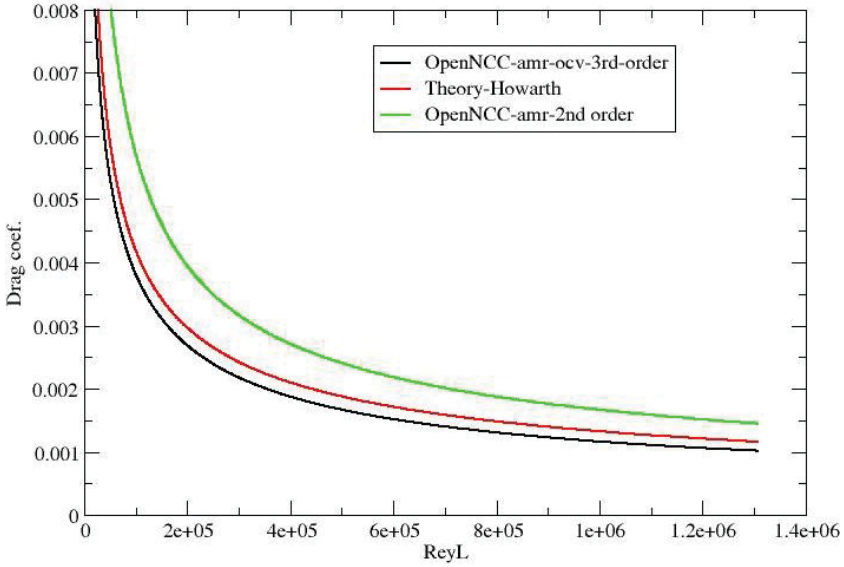

Figure 19 Skin coefficients along the flat plat.

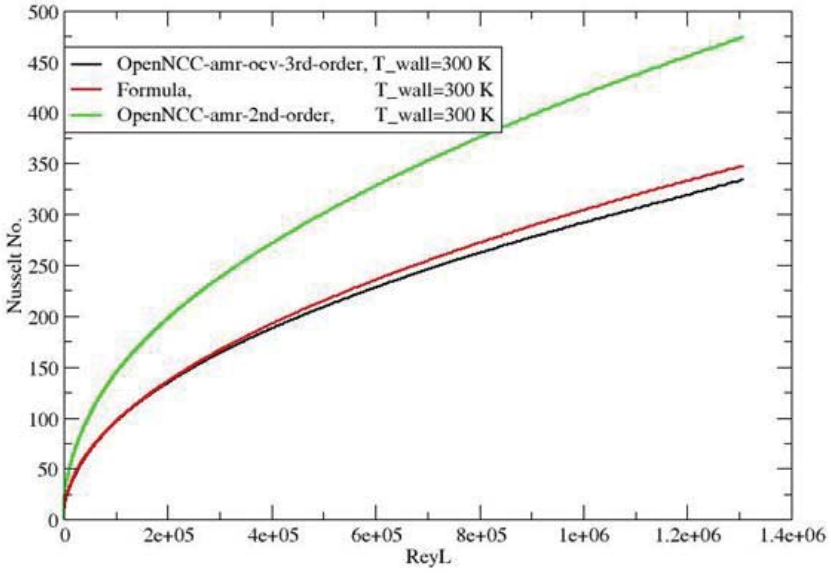

Figure 20 Nusselt numbers along the flat plate.

A Single-element LDI Combustor

A single-element LDI combustor is selected for the purpose of demonstration. This combustor consists of an air passage with a sixty-degree six-bladed air swirler, a converging-diversion section and a chamber with a square cross-section. The fuel is injected through the center of the swirler and exit at the throat of the venturi. The mesh consists of 1,653,265 polyhedrons, 9,524,206 faces and 1,837,619 nodes. The third order scheme without adaptive second order damping is selected.

The generalized wall function is applied to solid wall boundaries. The thermal boundary condition for all the solid surfaces of the combustor is set to be adiabatic. The RANS cubic turbulence model is used. The contours of the static pressure in the center plane of the geometry and iso-surfaces of low pressure are plotted in Figure 14. In Figure 15, the contours of the axial velocity in the center plane of the geometry and the iso-surfaces of low pressure are shown together. The precessing vortex core (PVC) that is represented by the low pressure iso-surfaces is quite noticeable. It can be contributed to the use of the third order scheme.

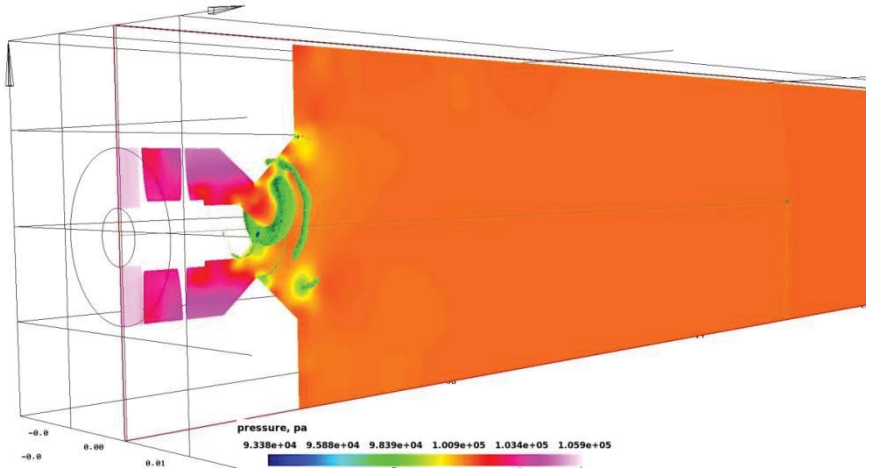

Figure 21 Static pressure contours and pressure iso-surfaces of non-reacting flow at z=0 plane.

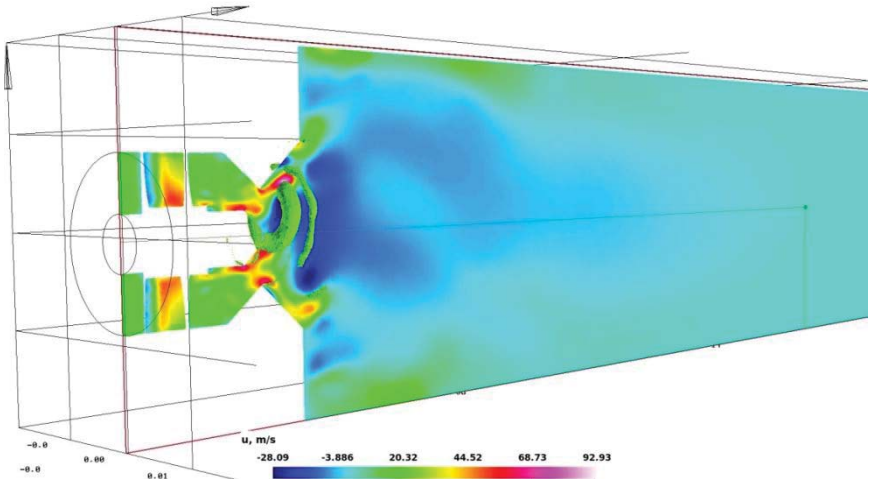

Figure 22 Axial velocity contours and pressure iso-surfaces of non-reacting flow at z=0 plane.

Preliminary Reacting Results

1. Conceptual N+3 Low NOx Combustor at low-power setting

The geometry represents a 12 degree sector of the combustor. At the inlet of the swirler, the mass flow rate and the static temperature of the gas phase are specified as 0.1875 kg/s and 545.1 K respectively. At the outflow boundary, the static pressure is imposed at 654266 Pa. The film cooling conditions from upper and lower walls are also applied. At the low power setting, only the pilot is burning at 0.132 kg C12H21, the liquid fuel, per minute. The chemical kinetics for the gaseous phase is represented by nineteen reactions and fourteen species, which consist of C12H21, O2, CO2, CO, H2O, N2, NO, O, OH, H2, H, N2O, N, and CH. Four sets of control volumes are selected for timing study. The first set of control volumes is the original mesh which contains 5,162,593 tetrahedrons.

The second set of control volumes is derived from the nodes of the original tetrahedrons. It contains 926,030 polyhedrons. A slice of the middle plane of the domain is shown in Figure 24. The third set of control volumes is the overlapping one by mesh-realignment process from the original tetrahedrons. It contains 5,445,835 polyhedrons and shown in Figure 26. The fourth set of control volumes is derived from the nodes and cells of the original tetrahedrons discussed in Ref. [4]. It contains 6,088,623 polyhedrons and its boundary polygons and mid-plane slice are shown in Figures 28 and 29. The stochastic injection option is turned on for all four cases and it will cause the behavior and pattern to be different because of its randomness. In Figures 23, 25, 27 and 30, the temperature contours of the reacting flow at mid-planes for four sets of cases are shown. In Table 1, brief timing information is listed. Since numbers of droplets in the domain are quite different when the spray solver achieves the equilibrium, the timing information is used as a reference.

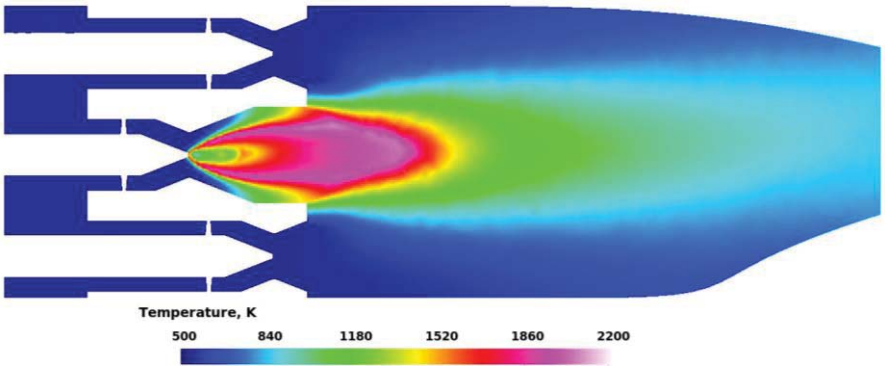

Figure 23 Temperature contours of reacting flow at z=0 plane: 5,162,593 tetrahedrons.

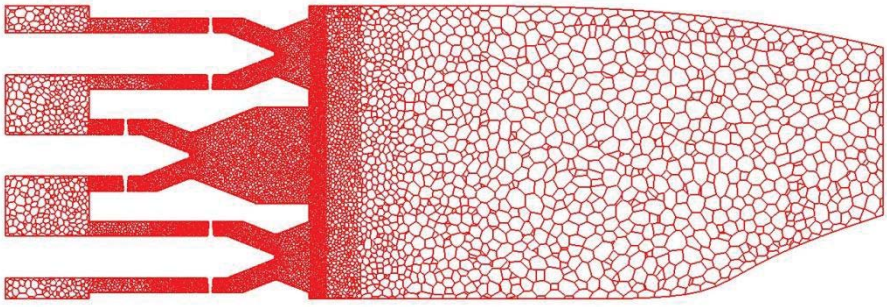

Figure 24 A slice of mesh-node-based control volumes: 926,030 polyhedrons.

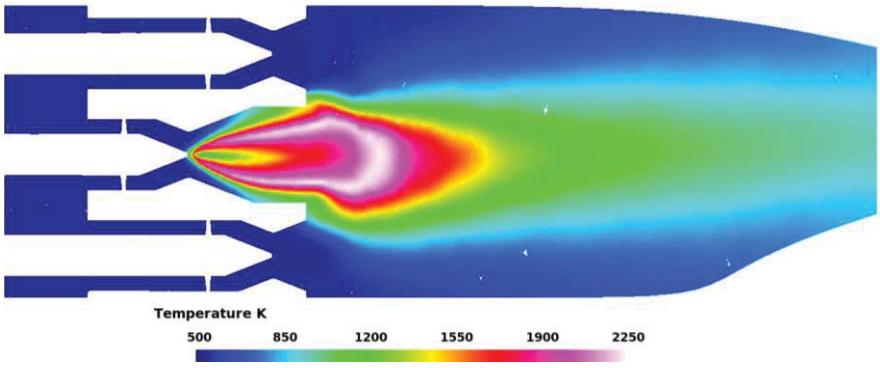

Figure 25 Temperature contours of reacting flow at z=0 plane.

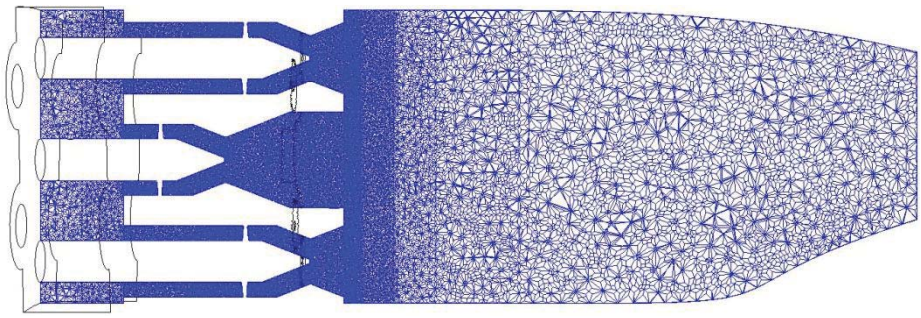

Figure 26 A slice of mesh-realigned overlapping control volumes: 5,445,835 polyhedrons.

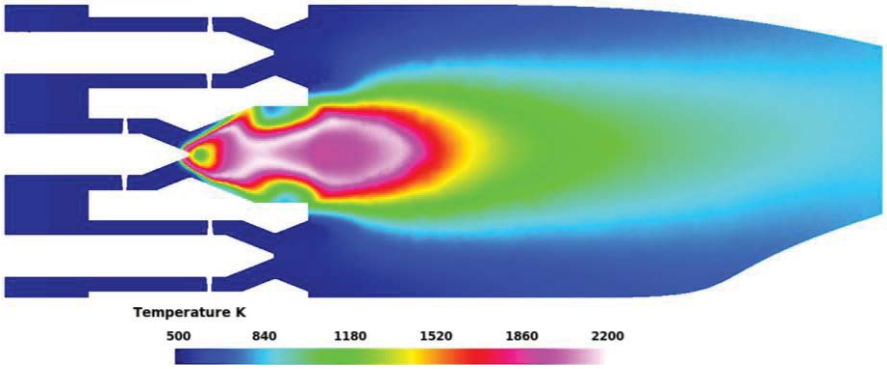

Figure 27 Temperature contours of reacting flow at z=0 plane. Third order scheme with second order adaptive damping is used.

Figure 28 Boundary polygons by mesh-node-and-cell based control volumes: 6,088,623 polyhedrons.

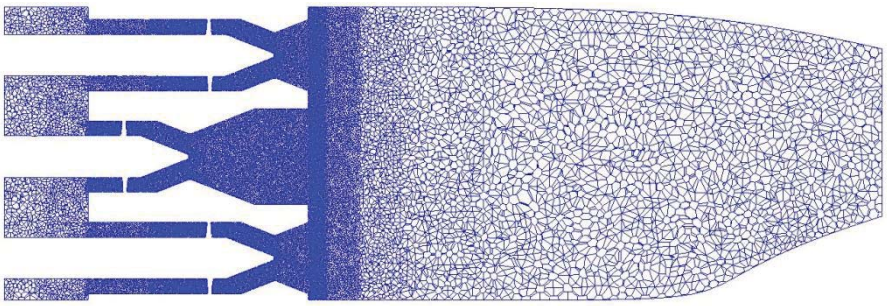

Figure 29 A slice of mesh-node-and-cell based control volumes: 6,088,623 polyhedrons.

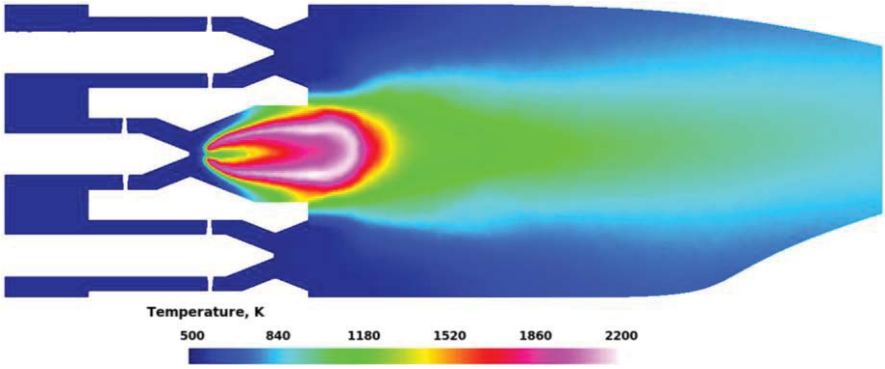

Figure 30 Temperature contours of reacting flow at z=0 plane.

Table 1Timing Study

Control volumes	Control surfaces	Iteration/second	Droplets in domain	Remark
5162593	10466807	0.40 (400 cores)	4348	
926030	6390318	0.39 (400 cores)	133802	
5445835	31542042	0.10 (400 cores)	97386	3rd order scheme
6088623	31896429	0.18 (400 cores)	155530	

2. Reacting Single-element LDI Case

Two sets of overlapping control volumes generated by mesh realignment process are selected for the simulations.
The first control volume which is derived from a set of tetrahedron-dominated hanging-node polyhedrons consists of 3,480,799 grid points, 19,374,250 faces and 2,737,973 cells. The second control volume which is derived from a set of all-hexahedron mesh consists of 694,847 grid points, 10,110,656 faces and 890,208 cells. Since the second original mesh contains many high aspect ratio hexahedrons, the mesh realignment process generates many control volumes with extreme small acute angles.

For reacting cases, in addition to the boundary conditions for the gaseous phase described above, the liquid fuel, C12H23, is injected into the computational domain from a pressure swirl injector. The diameter of the orifice is .0006 m. The fuel atomizer is set at a pressure 110kPa and delivers a flow rate of 0.025 kg/min. The spray has a 90 degree spray angle which is the same as the angle between the converging-diverging venturi

attached to the swirler. An initial droplet size distribution is prescribed to provide the liquid fuel injection condition,

$$\frac{dn}{n} = 4.21\times 10^{6}[\frac{d}{d_{32}}]^{3.5} e^{-16.98(\frac{d}{d_{32}})^{0.4}} \frac{dd}{d_{32}}$$

where n is the total number of the droplets and dn is the number of droplets in the size range between d and $d+dd$. This correlation also requires the specification of Sauter mean diameter, d_{32}, and the number of droplet classes. The equivalence ratio computed from the gaseous and liquid inlet boundary conditions is about 0.72. The adiabatic flame temperature is around 2100 K. The chemical kinetics for the gaseous phase is represented by five reactions and seven species, which consist of C12H23, O2, CO2, CO, H2O, N2 and NO.

TFNS results computed using third order scheme plus adaptive second order damping and the well-mixed combustion model for the overlapping control volumes, depicted in Figures 31(a) and 32(a), are shown for axial velocity and temperature in the center plane (i.e. z=0 plane), in Figure 31 and 32, respectively.

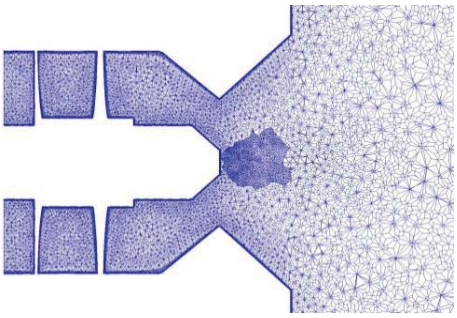

a

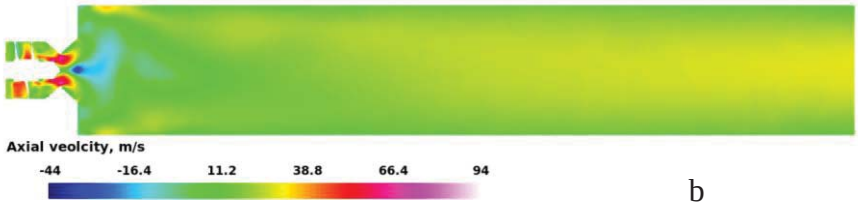

b

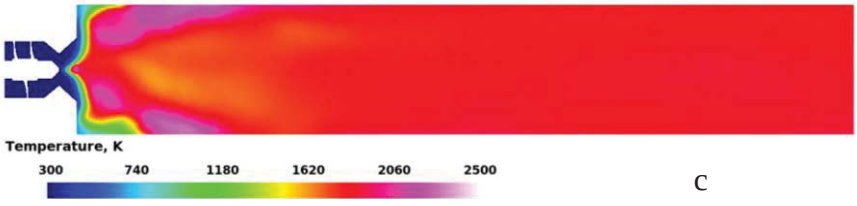

c

Figure 31 (a) overlapping control volumes (b) axial velocity (c) temperature

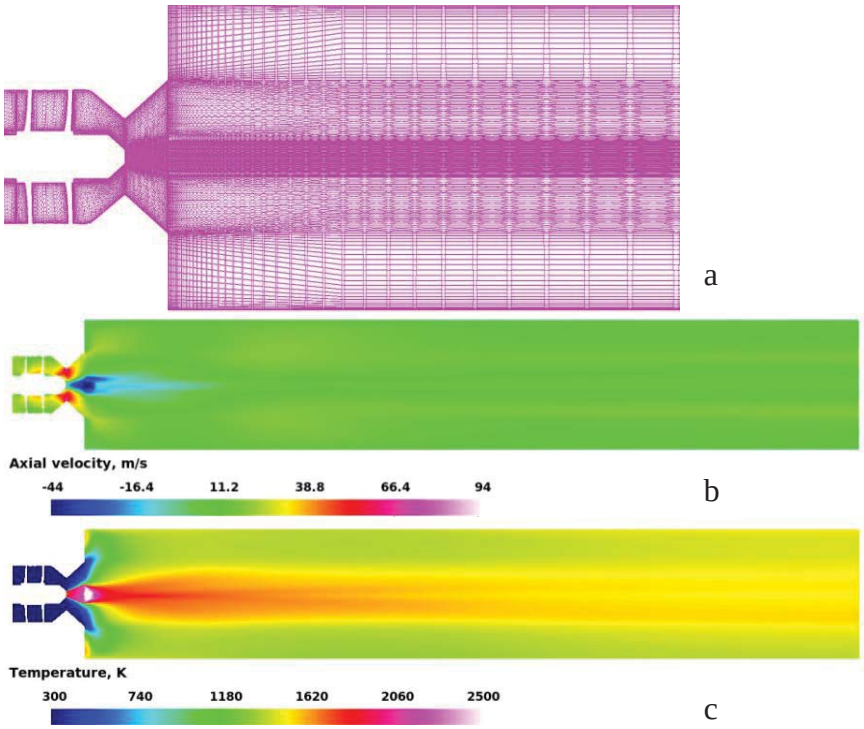

Figure 32 (a) overlapping control volumes (b) axial velocity (c) temperature

In Figure 32, the highest temperature of the flame is much larger than in Figure 31 case. It could be due to the existence of too many high aspect ratio control volumes in the case shown by Figure 32. It is also speculated that the third order scheme applied to the high gradient area might give rise to the overshoot of temperatures.

The time-averaged centerline axial velocity and the centerline temperature are presented in Figures 33 and 34, along with the measured data. The discrepancy between the computed values and the experimental data are noticeable.

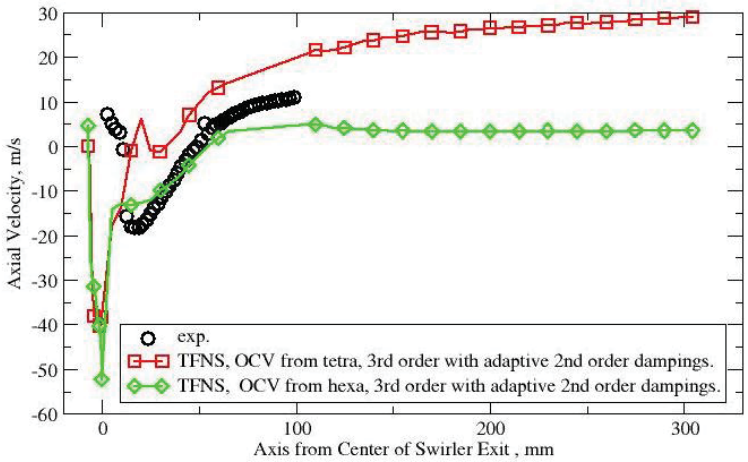

Figure 33 Comparison of the mean axial velocity along the center line.

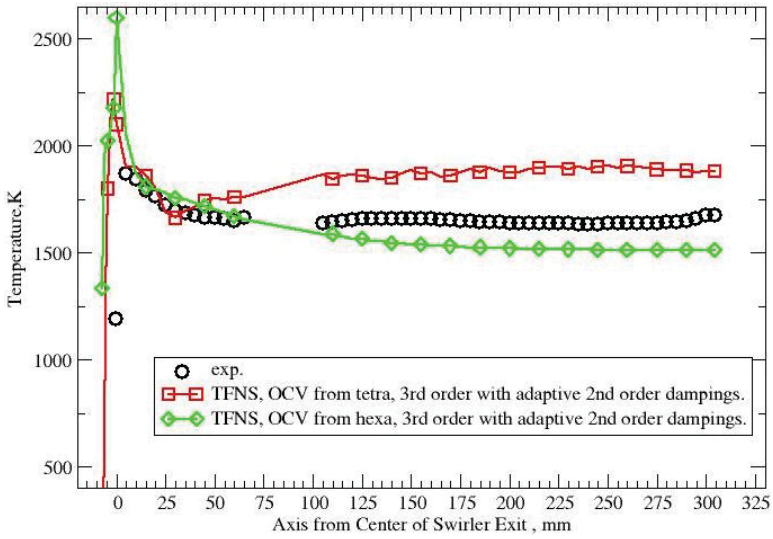

Figure 34 Comparison of the mean temperature along the center line.

Concluding Remarks

The capability of (1) generating control volumes anchored at the nodes of a mesh; and (2) generating staggered control volumes via mesh reconstructions, in terms of either mesh realignment or mesh refinement, is now implemented in a preliminary version of the OpenNCC, which is intended as the self-contained, releasable edition of the National Combustion Code (NCC). It is the third part of the adaptive mesh refinement option in OpenNCC.

A stand-alone single-element LDI combustor and a conceptual N+3 LDI combustor are selected for the demonstrations of generating the control volumes. The third order scheme through the usage of overlapping control volume is also implemented and benchmarked against a flat plat in the laminar flow. It is observed that the third order scheme with adaptive second order damping has the tendency of overshooting the temperature and velocity for the case of single–element LDI combustor when mesh-realigned overlapping control volumes are used.

Acknowledgements

This work is supported by the NASA Fundamental Aeronautics Program. The original mesh of the conceptual N+3 low NOx combustor is provided by Chris Heath from MDAO branch, NASA/GRC.

References

[1] Liu, N.-S., "Assessment and Improvement of Engineering Simulation for Multiphase Turbulent Combustion in a Lean Direct Injection Combustor," ISABE-2011-1108, 20th International Symposium on Air Breathing Engines, September 12-16, 2011, Gothenburg, Sweden.
[2] Liu, N.-S., Shih, T.-H., and Wey, C.T., "Numerical Simulations of Two-Phase Reacting Flow in a Single-Element Lean Direct Injection (LDI) Combustor Using NCC," NASA/TM-2011-217031, July 2011.
[3] Wey, T. and Liu, N.-S., "Simulation of a Single-Element Lean-Direct Injection Combustor Using Arbitrary Polyhedral Mesh," AIAA 2012-0204, 50th Aerospace Sciences Meeting and Exhibit January 9-12, 2012, Nashville, Tennessee.
[4] Liu, N.-S. and Wey, C.T., "On the TFNS Subgrid Models for Liquid-fueled Turbulent Combustion," AIAA 2014-3569, 50th AIAA/ASME/SAE/ASEE Joint Propulsion Conference, July 28-30, 2014, Cleveland, OH.
[5] Wey, T. C. and Liu, N.-S., "Simulation of a Single-Element Lean-Direct Injection Combustor Using a Polyhedral Mesh Derived from Hanging-Node Elements," AIAA 2013-0739, 51th AIAA ASM, Jan. 7-10, 2013, Grapevine, TX.
[6] Wey, T. C. and Liu, N.-S., "Updates to Simulation of a Single-Element Lean-Direct Injection Combustor Using a Polyhedral Mesh Derived from Hanging-Node Elements," AIAA 2014-1385, 52nd AIAA ASM, Jan. 13-17, 2014, National Harbor, MD.